Chinese Chemical Letters 35 (2024) 108704

Contents lists available at ScienceDirect

Chinese Chemical Letters

journal homepage: www.elsevier.com/locate/cclet

Enhanced electrochemical oxidation of perfluorooctanoic acid on Ti/SnO_2-Sb electrode by surface morphology regulation

Kaiqiang Hou[a], Genwang Zhu[a], Yujie Feng[b,*], Yanming Liu[a,*], Xie Quan[a]

[a] Key Laboratory of Industrial Ecology and Environmental Engineering (Ministry of Education, China), School of Environmental Science and Technology, Dalian University of Technology, Dalian 116024, China
[b] State Key Laboratory of Urban Water Resource and Environment, School of Environment, Harbin Institute of Technology, Harbin 150090, China

ARTICLE INFO

Article history:
Received 13 February 2023
Revised 26 May 2023
Accepted 19 June 2023
Available online 21 June 2023

Keywords:
Electrochemical oxidation
Nanoneedle SnO_2-Sb
Perfluoroalkyl compounds
Electrochemical degradation
Persistent organic pollutants

ABSTRACT

Electrochemical oxidation is an effective method to degrade persistent organic pollutants. However, due to the limited catalytic activity of traditional thin film electrodes, the anodic oxidation process is slow and usually requires high energy consumption. Herein, Ti/SnO_2-Sb electrode with regulated surface structure was reported to enhance the performance for electrochemical oxidation of persistent organic pollutants. The electrode deposited with SnO_2-Sb nanoneedles (Ti/N-SnO_2-Sb) showed higher oxidation activity. Its kinetic constant for perfluorooctanoic acid (PFOA) oxidation was 2.0 h^{-1} and the total organic carbon removal rate was 81.7% (4 h) at a relatively low current density of 6 mA/cm^2. Compared with Ti/SnO_2-Sb thin film and nanoparticles, Ti/N-SnO_2-Sb significantly improved the electrochemical active area and ·OH yield, and simultaneously reduced the electron transfer resistance, which enabled it to oxidize PFOA more rapidly even at a lower potential. This work provides a new strategy for promoting the electrochemical oxidation performance.

Long chain perfluoroalkyl compounds (PFCs) represented by perfluorooctanoic acid (PFOA) are typical persistent organic pollutants (POPs), which are chemically stable, highly toxic and easy to be bioaccumulated. PFCs has been widely detected in various environmental media [1,2], even in organisms [3–5] and drinking waters of many countries [6], posing great risks to the environment and human health. The kinetics for PFCs removal from water by traditional biological and chemical technologies is relatively poor [7], so it is urgent to develop efficient methods to degrade such contaminants. Electrochemical oxidation has attracted extensive research interest in POPs degradation because of its strong oxidation ability, mild and reagent free conditions and possibility of using renewable energy [8,9]. The anode material is one of the most important factors affecting its oxidation performance. Searching for highly active anode material is still desirable for electrochemical oxidation of POPs.

Many anode materials such as doped SnO_2 [10–12], doped diamond [13,14] and Ti_4O_7 [15–17] have been developed for electrochemical oxidation of PFCs. Among these anode materials, SnO_2 coated on Ti substrate (SnO_2/Ti) have been studied widely due to its advantages of easy preparation, low cost and high oxygen evolution potential. Although it has been found that doping metal (Sb, Ce, Pb, *etc.*) and halogen atoms can improve the catalytic activity and stability of Ti/SnO_2 electrode by changing its chemical composition [10–12], electrochemical oxidation of PFCs with Ti/SnO_2 is still limited by its slow kinetics and high energy consumption. At the same time, studies have proved that in addition to doping, the influence of electrode surface structure on catalytic performance is equally important. Some special morphology such as nanoneedle [18], nanorod [19–23] and nanoflower [24] can provide a larger active area and more catalytic sites, so they usually show better catalytic performance than thin film electrodes. More importantly, the nanoneedle tip can form a more concentrated electric field, resulting in accelerated charge transfer and concentrated reactants at the tip, which have showed improved performances for electrocatalytic reduction [25–28]. The electrodes with nanoneedle structures may overcome the limitations of slow kinetics and high energy consumption for traditional thin film electrode. However, the application of nanoneedle morphology in electrochemical oxidation of pollutants has not been reported.

Herein, a strategy of regulating surface structure was proposed to enhance the electrochemical oxidation performance of Ti/SnO_2-Sb electrode by using nanoneedle SnO_2-Sb (Ti/N-SnO_2-Sb). PFOA was selected as the target pollutant to evaluate the electrode performance. The Ti/N-SnO_2-Sb electrode showed enhanced PFOA ox-

* Corresponding authors.
E-mail addresses: yujief@hit.edu.cn (Y. Feng), liuyanm@dlut.edu.cn (Y. Liu).

https://doi.org/10.1016/j.cclet.2023.108704
1001-8417/

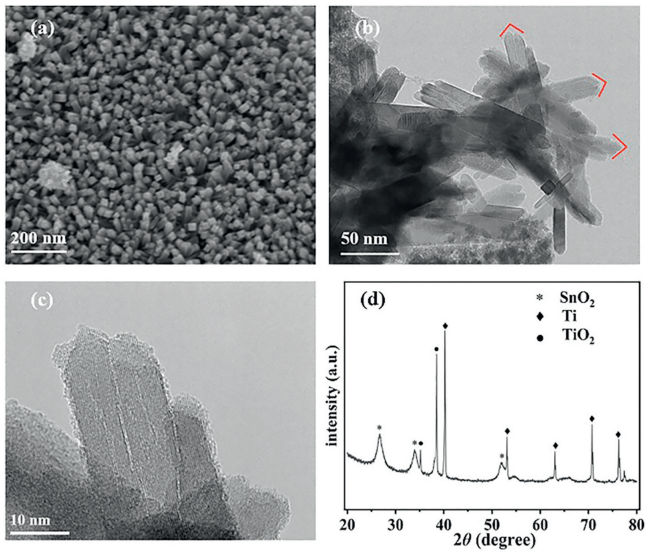

Fig. 1. (a) SEM image and (b, c) TEM images of N-SnO_2-Sb, (d) XRD spectrum of Ti/N-SnO_2-Sb.

idation kinetics and total organic carbon (TOC) removal efficiency as well as reduced energy consumption compared with Ti/SnO_2-Sb thin film and nanoparticles. The enhanced PFOA oxidation on Ti/N-SnO_2-Sb was originated from its accelerated charge transfer, improved electrochemical active area and $^{\bullet}OH$ yield due to the nanoneedle tip structure.

The N-SnO_2-Sb catalyst was synthesized by hydrothermal method, and Ti/N-SnO_2-Sb electrode was prepared by coating sol-gel derived SnO_2-Sb thin film on Ti (denoted as Ti/SnO_2-Sb), followed by electrophoresis of N-SnO_2-Sb catalyst. Fig. 1a and Fig. S1 (Supporting information) show the scanning electron microscopy (SEM) images of the synthesized N-SnO_2-Sb catalyst. The nanoneedles are vertically aligned on the sheet and completely cover the catalyst surface. The distribution of nanoneedles is dense and uniform. The transmission electron microscope (TEM) image confirms that N-SnO_2-Sb is consisted of nanoneedles with pyramid like tips (Fig. 1b). The length of the nanoneedles is about 50 nm, and the diameter is about 10 nm. High resolution TEM shows that these nanoneedles are high quality single crystals (Fig. 1c).

The SEM images in Fig. S2 (Supporting information) show the electrode surface morphology before and after electrophoresis, which reveal that N-SnO_2-Sb catalyst is uniformly dispersed on the surface of Ti/N-SnO_2-Sb electrode after electrophoresis. It proves that the N-SnO_2-Sb has been successfully deposited. The X-ray diffraction (XRD) spectrum (Fig. 1d) shows the lattice structure of Ti/N-SnO_2-Sb. The diffraction peaks at 26.6°, 33.8° and 38° can be assigned to the (110), (101) and (220) crystal planes of rutile SnO_2, originating from SnO_2-Sb nanoneedles and sol-gel thin film [11]. The other diffraction peaks are consistent with the characteristic peaks of TiO_2 and Ti substrate [14]. The Ti/SnO_2-Sb shows the same diffraction pattern and similar peak intensity as Ti/N-SnO_2-Sb (Fig. S3 in Supporting information), demonstrating their crystal structures are almost identical.

The electrochemical oxidation activity of Ti/N-SnO_2-Sb was evaluated by linear sweep voltammogram (LSV). It shows the current increases in the electrolyte with PFOA relative to that without PFOA at potential more negative than 1.8 V (*vs.* Ag/AgCl, Fig. 2a), which suggests Ti/N-SnO_2-Sb is active for PFOA oxidation. The PFOA oxidation on Ti/N-SnO_2-Sb and Ti/SnO_2-Sb electrodes were compared to verify the feasibility of tuning electrochemical performance by surface morphology modification. As shown in Fig. 2b, Ti/N-SnO_2-Sb exhibits higher PFOA removal efficiency than

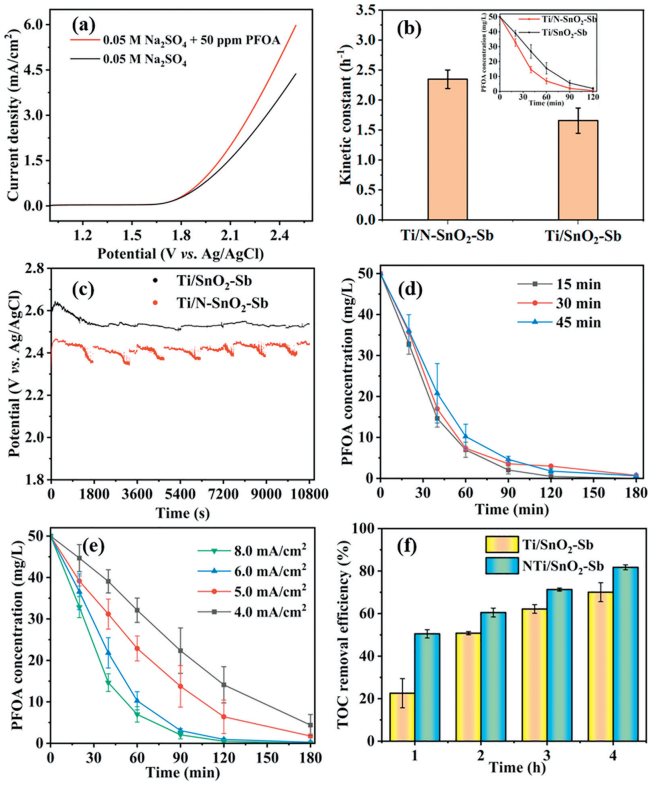

Fig. 2. (a) LSV curves of Ti/N-SnO_2-Sb in 0.05 mol/L Na_2SO_4 with and without PFOA, (b) kinetic constants and (c) chronopotentiometric curves for PFOA oxidation on Ti/N-SnO_2-Sb and Ti/SnO_2-Sb at 8.0 mA/cm^2, PFOA oxidation on Ti/N-SnO_2-Sb with (d) electrophoresis time of 15–45 min and (e) current densities of 4.0–8.0 mA/cm^2, (f) TOC removal efficiencies on Ti/N-SnO_2-Sb and Ti/SnO_2-Sb.

Ti/SnO_2-Sb at current density of 8.0 mA/cm^2. The first-order kinetic constant is 2.35 h^{-1} for PFOA degradation on Ti/N-SnO_2-Sb, greater than 1.66 h^{-1} for Ti/SnO_2-Sb, which proves that the deposited N-SnO_2-Sb can effectively enhance PFOA oxidation rate by regulating electrode surface morphology. It is worth noting that the real-time potential monitoring (Fig. 2c) shows the operating potential of Ti/N-SnO_2-Sb for PFOA oxidation (~2.45 V *vs.* Ag/AgCl) is decreased by about 100 mV compared with Ti/SnO_2-Sb (~2.55 V *vs.* Ag/AgCl). Since the chemical composition and crystal structure of the two electrodes are almost the same, the enhanced oxidation kinetics and reduced running potential of Ti/N-SnO_2-Sb could be attributed to its nanoneedle structure. The characteristic nanotips of Ti/N-SnO_2-Sb will effectively reduce the energy consumption for electrochemical oxidation, which is of great significance in practical applications.

The effects of electrophoresis parameters and current density on PFOA oxidation were investigated. The electrophoresis time may affect the catalyst loading. Therefore, PFOA oxidation was conducted on Ti/N-SnO_2-Sb electrodes prepared with different electrophoresis time. Fig. 2d shows the PFOA removal efficiency has no obvious change when the electrophoresis time is increased from 15 min to 45 min, indicating 15 min is long enough for depositing N-SnO_2-Sb. After 15 min deposition, it can be observed the electrode surface was completely covered by the N-SnO_2-Sb catalyst, so 15 min of electrophoresis was used for the following experiments. To investigate the influence of applied current density on PFOA degradation, electrochemical oxidation of PFOA on Ti/N-SnO_2-Sb was conducted at 4.0–8.0 mA/cm^2. As shown in Fig. 2e, its PFOA removal efficiency increases gradually as the current density increases from 4.0 mA/cm^2 to 8.0 mA/cm^2. The removal efficiency is 98.1% after electrochemical oxidation of 2 h

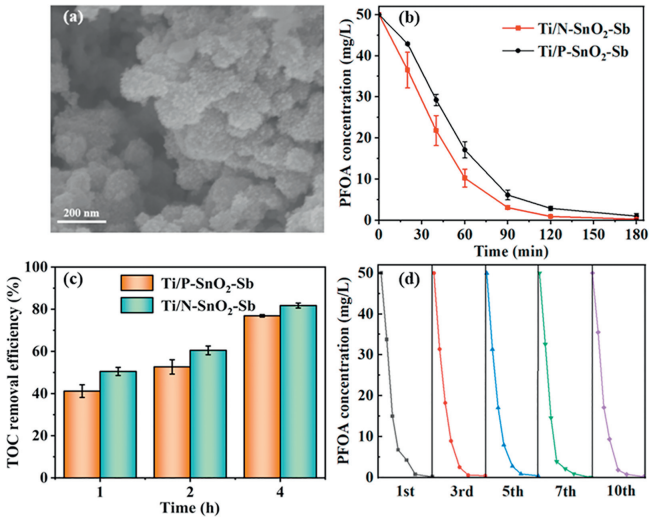

Fig. 3. (a) SEM image of P-SnO_2-Sb, (b) PFOA oxidation on Ti/N-SnO_2-Sb and Ti/P-SnO_2-Sb electrodes, (c) TOC removal efficiency and (d) 10 cycles of PFOA oxidation on Ti/N-SnO_2-Sb (6.0 mA/cm^2).

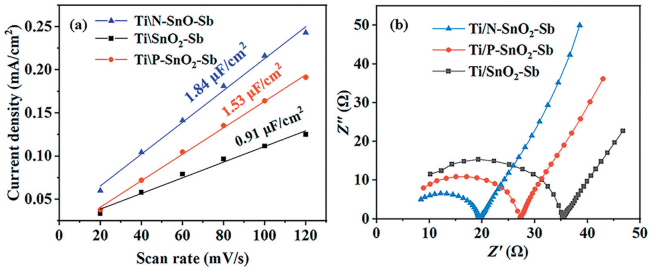

Fig. 4. (a) ECAS and (b) EIS of Ti/N-SnO_2-Sb, Ti/P-SnO_2-Sb and Ti/SnO_2-Sb electrodes.

at 6.0 mA/cm^2. The PFOA oxidation follows pseudo-first-order kinetics (Fig. S4 in Supporting information). Its kinetic constant for PFOA oxidation increases significantly from 0.95 h^{-1} at 5.0 mA/cm^2 to 2.00 h^{-1} at 6.0 mA/cm^2. Although the kinetic constant further increases to 2.35 h^{-1} at 8.0 mA/cm^2, the rate increase becomes less pronounced compared with that from 5.0 mA/cm^2 to 6.0 mA/cm^2. Thus 6.0 mA/cm^2 was used for the following experiments. At 6.0 mA/cm^2, its kinetic constant is comparable or even higher than those of doped SnO_2-Sb [12], doped PbO_2 [9,29], B doped diamond [13,30] and Ti_4O_7 [16] electrodes (0.40–2.22 h^{-1}, Table S1 in Supporting information).

The total organic carbon (TOC) removal rate was further measured to verify the role of N-SnO_2-Sb for PFOA mineralization. Fig. 2f shows the TOC removal efficiency for electrochemical oxidation of PFOA on Ti/N-SnO_2-Sb and Ti/SnO_2-Sb electrodes. After electrochemical oxidation of PFOA at relatively low current density (6.0 mA/cm^2) for 2–4 h, the TOC removal efficiencies are 60.5%–81.7% for Ti/N-SnO_2-Sb, which proves the Ti/N-SnO_2-Sb electrode is efficient for decomposing PFOA to CO_2 at low current density. As expected, Ti/N-SnO_2-Sb shows higher TOC removal efficiency than Ti/SnO_2-Sb. These results suggest the nanoneedle structure can facilitate PFOA mineralization and reduce the accumulation of organic intermediates.

In order to further investigate the influence of catalyst morphology on PFOA oxidation, SnO_2-Sb without nanoneedles were synthesized by hydrothermal method and deposited on Ti/SnO_2-Sb by electrophoresis (denoted as Ti/P-SnO_2-Sb). The SEM and TEM images (Fig. 3a and Fig. S5 in Supporting information) show the uniform distribution of P-SnO_2-Sb nanoparticles on the electrode surface. The nanoparticles are composed of short nanorods. Nanoneedle cannot be observed. In the XRD spectrum (Fig. S3), Ti/P-SnO_2-Sb has the same diffraction peaks as Ti/N-SnO_2-Sb, and their peak intensity is approximately the same, suggesting Ti/P-SnO_2-Sb and Ti/N-SnO_2-Sb have identical crystal structure. Their performance for electrochemical oxidation of PFOA was compared at 6 mA/cm^2. As shown in Fig. 3b, Ti/N-SnO_2-Sb exhibits higher PFOA removal efficiency than Ti/P-SnO_2-Sb, and its PFOA oxidation rate constant (2.00 h^{-1}) is 1.32 times as great as that of Ti/P-SnO_2-Sb electrode (1.51 h^{-1}) (Fig. S6 in Supporting information), implying that the nanoneedle structure endows Ti/N-SnO_2-Sb electrode with higher activity for electrochemical oxidation of PFOA. The electrical energy for PFOA concentration reduced by one order of magnitude was 17.8 kWh/m^3 for Ti/N-SnO_2-Sb, which was reduced 1.8 times compared with Ti/SnO_2-Sb. It is worth noting the energy consumption of Ti/N-SnO_2-Sb is much lower than the reported SnO_2-Sb, PbO_2, B doped diamond and Ti_4O_7 electrodes mentioned above (58.5–180 kWh/m^3, Table S1), indicating that Ti/N-SnO_2-Sb has reduced energy consumption among these electrodes.

The TOC removal rates at Ti/N-SnO_2-Sb and Ti/P-SnO_2-Sb were compared in Fig. 3c, which shows Ti/N-SnO_2-Sb has higher TOC removal efficiency, confirming Ti/N-SnO_2-Sb is superior to Ti/P-SnO_2-Sb for PFOA mineralization. The stability of Ti/N-SnO_2-Sb for electrochemical oxidation of PFOA was tested through 10 consecutive batch degradation experiments (6.0 mA/cm^2). Its PFOA removal efficiency exhibits no obvious change during 10 cycles of PFOA degradation experiments (Fig. 3d), implying that the Ti/N-SnO_2-Sb electrode is stable and reusable for electrochemical oxidation of PFOA.

To get insight into the better performance of Ti/N-SnO_2-Sb for electrochemical oxidation of PFOA, the factors contributed to the electrochemical activity were investigated. Considering the catalyst morphology may influence the electrochemical active surface area (ECAS), the double-layer capacitances which are linear to ECAS were measured for Ti/N-SnO_2-Sb, Ti/P-SnO_2-Sb and Ti/SnO_2-Sb electrodes (Fig. S7 in Supporting information). As shown in Fig. 4a, the double-layer capacitance of Ti/N-SnO_2-Sb is 1.84 μF/cm^2, which is 2.0 times as great as that of Ti/SnO_2-Sb (0.91 μF/cm^2), revealing ECAS is increased after electrophoresis of N-SnO_2-Sb catalyst. Compared with Ti/P-SnO_2-Sb, Ti/N-SnO_2-Sb presents 1.2 times higher double-layer capacitance (1.53 μF/cm^2). The higher ECAS of Ti/N-SnO_2-Sb could be contributed from its nanoneedle structure. The larger ECAS can provide more adsorption and reaction sites for PFOA oxidation, and thereby enhance PFOA degradation, which may be one of the reasons why Ti/N-SnO_2-Sb has better electrochemical oxidation performance.

The electrode morphology will change its electric field distribution and charge transfer resistance [31]. It is generally believed that electrochemical oxidation of PFOA begins with transfering one electron to anode [32]. The charge transfer will affect PFOA oxidation performance. Here electrochemical impedance spectrum (Fig. 4b) was employed to test charge transfer resistance. Compared with the original Ti/SnO_2-Sb electrode, the charge transfer resistances of the electrodes with electrophoretic catalysts are reduced, and Ti/N-SnO_2-Sb shows the fastest charge transfer. For N-SnO_2-Sb, its unique curvature nanotips enhance the local electric field and distribute the potential more intensively, which endow faster electron transfer rate. Therefore, the interfacial polarization induced from high-curvature nanotips promotes its performance for PFOA degradation. The reduced charge transfer resistance also explains the phenomenon that the operating voltage of Ti/N-SnO_2-Sb electrode decreases.

The electrochemical degradation of organic pollutants on SnO_2-Sb electrode usually occurs *via* reactive oxygen species [13,32]. Herein electron paramagnetic resonance (EPR) was used to deter-

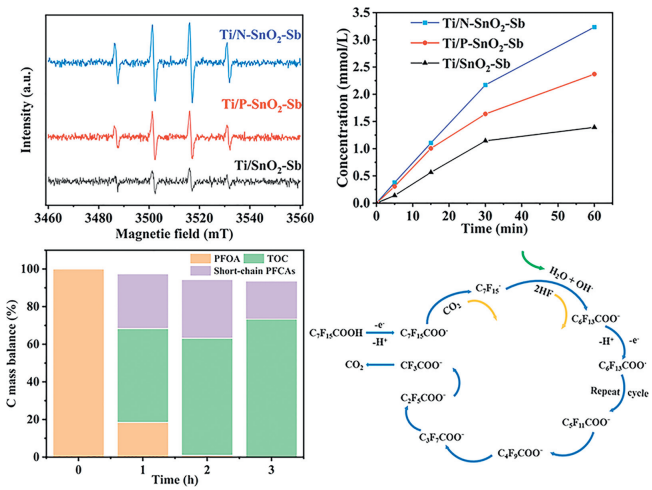

Fig. 5. (a) EPR spectra and (b) yields of ·OH generated on Ti/N-SnO_2-Sb, Ti/P-SnO_2-Sb and Ti/SnO_2-Sb, (c) carbon mass balance during PFOA oxidation on Ti/N-SnO_2-Sb electrode at 6.0 mA/cm^2, (d) possible pathway for PFOA oxidation.

mine the possible reactive oxygen species responsible for PFOA oxidation. The identified species is ·OH for the three electrodes, as revealed by the EPR spectra in Fig. 5a. After working for 10 min (0.05 mol/L Na_2SO_4, 6.0 mA/cm^2), the signal intensities of ·OH generated on Ti/N-SnO_2-Sb and Ti/P-SnO_2-Sb are greater than that on Ti/SnO_2-Sb, which proves that the electrodes with electrophoretic catalysts generate more ·OH. The ·OH concentration was measured with salicylic acid as probe compound (Fig. 5b). It confirms Ti/N-SnO_2-Sb and Ti/P-SnO_2-Sb have higher ·OH yields. More importantly, the ·OH yield on Ti/N-SnO_2-Sb is the highest, which can explain its fastest PFOA oxidation kinetics. PFOA oxidation with the presence of *tert*–butanol (·OH scavenger) indicates that ·OH was mainly responsible for PFOA degradation (Fig. S8 in Supporting information). Since the crystal structure of the three electrodes is almost the same, the difference in ·OH production ability should be attributed to the surface morphology regulation of SnO_2-Sb. The high-curvature nanotips of Ti/N-SnO_2-Sb electrode provide interfacial polarization field to accelerate electron transfer, concentrate reactants and promote ·OH generation, resulting in enhanced PFOA oxidation.

The intermediate products for electrochemical oxidation of PFOA on Ti/N-SnO_2-Sb were analyzed by HPLC-triple quadrupole mass spectrometer (Table S2 in Supporting information). The detected intermediates were short-chain perfluorocarboxylic acids (C2-C7). Fig. S9 (Supporting information) shows the concentrations of these short-chain intermediates as a function of reaction time. The concentrations of C2-C7 intermediates start to decrease after electrochemical oxidation of PFOA for 1 h or 2 h, and there is no high concentration of C2-C7 residues in the solution after 3 h. The monitored solution pH (Fig. S10 in Supporting information) indicates that perfluorocarboxylic acids exist as anions. The carbon mass balance was calculated and shown in Fig. 5c. A high carbon recovery rates of 93.5%–97.5% are obtained during 3 h of PFOA oxidation on Ti/N-SnO_2-Sb electrode, suggesting the main organic intermediates have been detected. Based on the above analysis and previous works [14], the possible pathway for PFOA oxidation was proposed in Fig. 5d. The PFOA is converted to $C_7F_{15}^{\bullet}$ *via* transferring one electron to Ti/N-SnO_2-Sb electrode and decarboxylation. The $C_7F_{15}^{\bullet}$ is oxidized by ·OH produced on Ti/N-SnO_2-Sb. Due to the instability of $C_7F_{15}OH$, it transfers to $C_6F_{13}COO^-$ *via* intramolecular rearrangement and hydrolysis. It can be converted to $C_5F_{11}COO^-$ *via* the above CF2 unzipping reactions, and the unzipping reactions will continue to occur until PFOA are oxidized to CO_2.

In summary, nanoneedle structured Ti/N-SnO_2-Sb was prepared by hydrothermal and electrophoresis method. It showed high activity and low energy consumption for electrochemical oxidation of PFOA with kinetic constant of 2.0 h^{-1} and energy consumption of 17.8 kWh/m^3, outperforming Ti/SnO_2-Sb thin film and nanoparticles. Moreover, its energy consumption was much lower than electrodes reported. The TOC removal efficiency was 81.7% in 4 h at relatively low current density of 6.0 mA/cm^2. The superior performance for Ti/N-SnO_2-Sb electrode was attributed to its larger electrochemical active area, faster charge transfer rate and higher •OH yield. Its curvature nanotips can enhance the local electric field and concentrate reactants at the electrode surface. This work provides a promising strategy to enhance the performance for electrochemical water treatment.

Declaration of competing interest

The authors declare that they have no known competing financial interests or personal relationships that could have appeared to influence the work reported in this paper.

Acknowledgments

This work was supported by Liaoning Revitalization Talents Program (No. XLYC2007069), the National Natural Science Foundation of China (Nos. 22076019 and 22222601) and open project of State Key Laboratory of Urban Water Resource and Environment, Harbin Institute of Technology (No. HC201705).

Supplementary materials

Supplementary material associated with this article can be found, in the online version, at doi:10.1016/j.cclet.2023.108704.

References

[1] J. Garnett, C. Halsall, A. Vader, et al., Environ. Sci. Technol. 55 (2021) 11049–11059.
[2] J.P. Benskin, L. Ahrens, D.C.G. Muir, et al., Environ. Sci. Technol. 46 (2012) 677–685.
[3] K. Huang, Y. Li, D. Bu, et al., Environ. Sci. Technol. Lett. 9 (2022) 147–152.
[4] L.Y. Meng, Y. Lu, Y.J. Wang, et al., ACS ES T Water 2 (2021) 195–205.
[5] W. Jouanneau, D. Léandri-Breton, A. Corbeau, et al., Environ. Sci. Technol. 56 (2022) 6091–6102.
[6] P.B. McMahon, A.K. Tokranov, L.M. Bexfield, et al., Environ. Sci. Technol. 56 (2022) 2279–2288.
[7] G.J. Yang, N. Zhang, J.N. Yang, et al., Water Res. 169 (2020) 115249.
[8] J. Radjenovic, N. Duinslaeger, S.S. Avval, et al., Environ. Sci. Technol. 54 (2020) 14815–14829.
[9] J.F. Niu, H. Lin, J.L. Xu, et al., Environ. Sci. Technol. 46 (2012) 10191–10198.
[10] H. Lin, J.F. Niu, J.L. Xu, et al., Environ. Sci. Technol. 47 (2013) 13039–13046.
[11] B. Yang, C.J. Jiang, G. Yu, et al., J. Hazard. Mater. 299 (2015) 417–424.
[12] Q.F. Zhuo, S.B. Deng, B. Yang, et al., Environ. Sci. Technol. 45 (2011) 2973–2979.
[13] C.E. Schaefer, S. Choyke, P.L. Ferguson, et al., Environ. Sci. Technol. 52 (2018) 10689–10697.
[14] Y.M. Liu, X.F. Fan, X. Quan, et al., Environ. Sci. Technol. 53 (2019) 5195–5201.
[15] H. Lin, R.L. Xiao, R.Z. Xie, et al., Environ. Sci. Technol. 55 (2021) 2597–2607.
[16] D.H. Huang, K.X. Wang, J.F. Niu, et al., Environ. Sci. Technol. 54 (2020) 10954–10963.
[17] G.S. Liu, Z. Zhou, J. Teng, et al., Chem. Eng. J. 371 (2019) 7–14.
[18] Y. Chen, G. Zhang, H.J. Liu, et al., ACS Catal. 22 (2022) 14376–14386.
[19] X.W. Xie, Y. Li, Z.Q. Liu, et al., Nature 458 (2009) 769 769.
[20] D. Bao, Q. Zhang, F.L. Meng, et al., Adv. Mater. 29 (2017) 1604799.
[21] Y.P. Zhu, Y.P. Liu, T.Z. Ren, et al., Adv. Funct. Mater. 25 (2015) 7337–7347.
[22] X.F. Liu, Z.P. Xing, Y. Zhang, et al., Appl. Catal. B: Environ. 201 (2017) 119–127.
[23] X.Y. Zhao, J. Meng, Z.H. Yan, et al., Chin. Chem. Lett. 30 (2019) 319–323.
[24] R.P. Hu, X. Xiao, S.H. Tu, et al., Appl. Catal. B: Environ. 163 (2015) 510–519.
[25] M. Liu, Y.J. Pang, B. Zhang, et al., Nature 537 (2016) 382–386.
[26] P. Liu, B. Chen, C.W. Liang, et al., Adv. Mater. 33 (2021) 2007377.
[27] J. Li, S. Chen, F.J. Quan, et al., Chem 6 (2021) 885–901.
[28] J.W. Li, J.N. Pan, W.N. Yin, et al., Chin. Chem. Lett. 34 (2023) 108049.
[29] H. Lin, J.F. Niu, J.S.T. Liang, et al., Sci. Total Environ. 579 (2017) 1600–1607.
[30] C.E. Schaefer, C. Andaya, A. Burant, et al., Chem. Eng. J. 317 (2017) 424–432.
[31] F.Y. Gao, S.J. Hu, X.L. Zhang, et al., Angew. Chem. Int. Ed. 59 (2020) 8706–8712.
[32] J.F. Niu, H. Lin, C. Gong, et al., Environ. Sci. Technol. 47 (2013) 14341–14349.